Proceedings of the 49th International School and Conference on the Physics of Semiconductors "Jaszowiec 2021"

Low-Temperature Cathodoluminescence of Nitrogen-Doped ZnO Films Deposited at Low-Temperature by Atomic Layer Deposition

M. Sarwar*, B.S. Witkowski, A. Sulich and E. Guziewicz

Institute of Physics, Polish Academy of Sciences,
Aleja Lotników 32/46, PL-02 668 Warsaw, Poland

Doi: 10.12693/APhysPolA.141.135 *e-mail: sarwar@ifpan.edu.pl

ZnO and ZnO:N films grown by atomic layer deposition and post-growth annealed were studied by scanning electron microscopy, low-temperature cathodoluminescence and X-ray diffraction. Low-temperature cathodoluminescence spectra reveal donor-related emission centered at 3.35 eV and acceptor-related emission centered at 3.31 eV. The cathodoluminescence maps recorded from the films cross-section clearly show the acceptor and donor-related emission coming from separate regions. The intensity of acceptor- and donor-related emission after annealing at different temperatures and media was studied. A comparison of the cathodoluminescence images, grain size and dislocation density indicates that the acceptor-related emission is not related to grain boundaries.

topics: zinc oxide, nitrogen doped zinc oxide, acceptor doping, low-temperature cathodoluminescence

1. Introduction

Zinc oxide, with a wide and direct bandgap (3.37 eV), has many potential applications as in electronic devices [1]. The main obstacle in extending the scope of ZnO to optoelectronics is the lack of stable, repeatable and reliable *p*-type ZnO. Interstitial H impurity and native defects as zinc interstitial, Zn_i, create abundant shallow donor states which are responsible for a high level of background electron conductivity, while oxygen vacancy V_O, and/or its complexes as Zn_iV_OH or nZn_iV_O create deep donor states responsible for the self-compensation effect. All these phenomena cause difficulties in converting conductivity to the *p*-type [2–5].

Acceptor dopants for ZnO include group I elements substituted for Zn or group V elements as oxygen substitutes. Group I elements, due to their small size, tend to occupy the interstitial sites where they act as donors. Group V elements with atomic number higher than oxygen tend to occupy antisite positions where they are donors [6]. Among the group V elements, nitrogen is the most suitable acceptor candidate due to the similarity of atomic size and electronic configuration to oxygen [7]. Nitrogen also acts as a shallow acceptor dopant for other II–VI compounds like ZnSe [8]. However, based on Density Functional Theory (DFT) calculations, substitutional nitrogen (N_O) is a deep acceptor in ZnO with the ionization energy of 1.3 eV [9], so it cannot be activated at room temperature.

Recently performed DFT investigations supported by experimental reports indicate that acceptor states in N-doped ZnO originate from complexes involving zinc vacancy, such as $N_O{\cdot}V_{Zn}$, $N_O{\cdot}V_{Zn}{\cdot}H$, and/or $V_{Zn}{\cdot}H$ [10–13]. In the light of these studies, oxygen-rich growth conditions that reduce the formation energy of zinc vacancy [4] are vital for the effective acceptor doping of zinc oxide, because the $V_{Zn}H$ and $V_{Zn}N_OH$ complexes that provide shallow acceptor states can be effectively created.

We have previously reported on *p*-type ZnO by nitrogen doping achieved using Atomic Layer Deposition (ALD) at a low growth temperature (100°C), which in the case of ALD provides oxygen-rich growth conditions. Measurement of RT Hall confirmed activation of acceptor doping after post-growth rapid thermal annealing (RTA) in oxygen at 800–900°C [14]. High-resolution cathodoluminescence (CL) revealed a complicated spatial distribution of donor and acceptor-related emissions across these *p*-type ZnO:N films [6]. In the present work, we investigate the influence of different ambiences and temperatures of RTA used for the activation of acceptor dopants on the intensity of acceptor-related CL of ZnO and ZnO:N films. The investigations are aimed at establishing the optimal annealing conditions and to find out whether acceptor-related emission is related to grain boundaries, as suggested in some previous studies [15].

TABLE I

Structural parameters of as-grown ZnO, ZnO:N and annealed ZnO:N calculated from X-ray diffractograms. Note: *Normalized integral area was calculated taking into account relative intensities mentioned in the JCPDS data file (file No. 36-1451).

Sample	Crystallite size [nm]			Normalize integral area* [%]			δ_{avg} (10^{10}
	[100]	[110]	[002]	[100]	[110]	[002]	[lines/cm^2]
ZnO as-grown	54.6 ± 1.4	41.7 ± 0.4	45.0 ± 0.3	8.44	83.42	8.13	5.40 ± 0.08
ZnO:N as-grown	73.6 ± 1.2	50.6 ± 0.3	–	19.44	80.55	–	3.49 ± 0.04
ZnO:N RTP O_2 800°C	75.8 ± 1.2	86.5 ± 1.3	–	18.10	81.89	–	1.40 ± 0.02
ZnO:N RTP N_2 400°C	47.5 ± 0.3	62.9 ± 0.3	–	19.00	80.90	–	2.88 ± 0.01

2. Experimental details

ZnO and ZnO:N films were grown on highly resistive silicon substrates at 100°C by using ALD. Before deposition, the substrates were cleaned by ultrasonication in acetone, isopropyl alcohol and then rinsed off by deionized water. The precursors for zinc and oxygen were diethylzinc (DEZn, $Zn(C_2H_5)_2$) and deionized water (DI). Ammonia water (NH_4OH, 25% ammonium hydroxide) was used as a nitrogen precursor at every fourth ALD cycle, resulting in nitrogen incorporation at the level of 10^{19} at/cm^3. A Savannah-100 reactor with pulsing time of 0.015 s and purging time of 2 s was used for all precursors. With 10000 ALD cycles, a film thickness of about 2 μm was obtained. RTA processes were performed in an Accu Thermo AW610 system from Allwin21 Inc. in O_2 at 800°C (for 3 min and 6 min) and in N_2 at 400°C (for 4 min). Structural analysis of the films was done by Cu $K_{\alpha 1}$ radiation (λ = 1.5406 Å) using a Bragg–Brentano powder diffractometer (X'Pert Pro Alpha1MPD from Philips/PANalytical) equipped with an incident beam Ge(111) Johansson monochromator and a strip detector. Cross-sectional scanning electron microscopy (SEM) images along with low-temperature (5.3 K) cathodoluminescence maps were recorded by a Hitachi SU-70 system synchronized with Gatan MonoCL-3 system, respectively.

3. Structural properties

X-ray diffractograms (XRD) showed polycrystalline nature for all the investigated films (Fig. 1). As grown ZnO showed the most intensive reflection at 56.5°, which corresponded to the [110] orientation of the crystallites with the presence of the [100] orientation of crystallites observed at 31.7° and the 002 reflection at 34.4° coming from the crystallites oriented along the [001] direction with the lower intensity. It is to be noted here that 001 transition is forbidden so we can observe the crystallites showing the [001] orientation by 002 reflection.

After nitrogen doping, the intensity of the peaks corresponding to orientations [110] and [100] decreased while 002 reflection disappeared. After all types of ZnO:N annealing were performed, the intensity of the X-ray reflections corresponding to

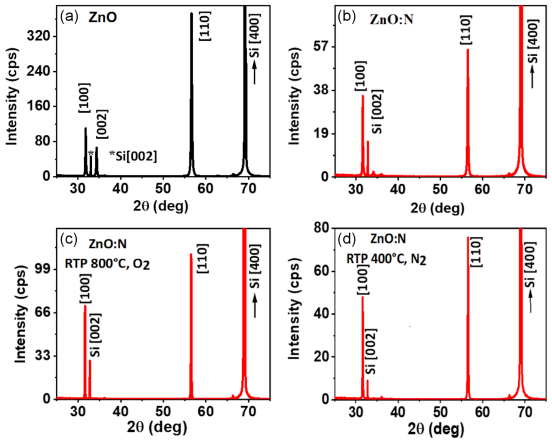

Fig. 1. X-ray diffractograms of as grown ZnO (a), as grown ZnO:N (b), ZnO:N annealed in O_2 at 800°C (c), ZnO:N annealed in N_2 at 400°C (d).

the orientations [110] and [100] relatively increased, however the [001] orientation did not appear. It should be noticed that the signal from the 002 reflection coming from the [001] crystallographic orientation in as-grown ZnO was quite weak (Fig. 1a) as compared to the peaks corresponding to the [100] and [110] orientations. As has been shown in our previous papers [16, 17], the low intensity diffraction peaks have tendency to disappear after annealing in favor of the most intensive, which also become narrower, indicating an increase in the size of the corresponding crystallites. Similar effects were observed here according to the values shown in Table I.

The proportion of the integral area [%] of the peaks is similar after both doping and annealing as shown in Table I. The crystallite size calculated using the Scherrer formula revealed that after doping with nitrogen, the crystallite size corresponding to the [110] orientation has increased from 41.7 nm to 50.6 nm, and for the [100] orientation it increased from 54.6 to 73.6 nm. After annealing of ZnO:N in O_2 at 800°C for 3 min, the size of the crystallites corresponding to the [110] has grown to 86.5 nm, while the size of crystallites oriented along the [100] orientation is 75.8 nm, so very close to the pre-RTP value. ZnO:N films annealed in N_2

at 400°C for 4 min show an increase of the crystallite size to 62.9 nm for the privilege orientation [110], while for the [100] it has decreased to 47.5 nm, so it is smaller compared to the as-grown ZnO and ZnO:N.

Dislocation density (δ) is an important parameter for assessing the structural quality and the structural defects in single-crystalline materials. The XRD microbeam studies of cold-worked metals involved the use of dislocation density at first [18]. Microbeam experiments indicated that dislocations lie at the boundary between two adjacent blocks, and metal is broken in between. Considering these conventions, the dislocation density can be calculated by the relation $\delta = n/D^2$, where δ represents dislocation density, n equals to 1 for isotropic distribution of dislocations, and D stands for the dimension of the block [19]. This relation was elaborated and further used for non-metallic single crystalline materials and epitaxial films where the same denoted D represents crystallite size. For polycrystalline materials, this relation does not exactly determine the dislocation density as the requirements of the model are not fully met. However the δ value, depending on the crystallite size, can be considered as a factor that describes the structural quality of polycrystalline films and has been used to evaluate polycrystalline layers [19, 16], also polycrystalline ZnO films [20]. In polycrystalline films, where few crystallographic orientations appears at the diffractograms with similar intensity, the value of δ can be calculated for every orientation separately, and the weighted average δ value accounts for crystallographic quality of the layer. For the ZnO films investigated here, the δ_{avg} was calculated as

$$\delta_{\text{avg}} = \delta_{100}\, I_{100}^{\text{norm}} + \delta_{110}\, I_{110}^{\text{norm}} + \delta_{002}\, I_{002}^{\text{norm}}, \quad (1)$$

where

$$\delta_{100} = \frac{1}{D_{100}^2}, \quad \delta_{110} = \frac{1}{D_{110}^2}, \quad \delta_{002} = \frac{1}{D_{002}^2} \quad (2)$$

and I_{100}^{norm}, I_{110}^{norm} and I_{002}^{norm} are the relative integrated intensities of the XRD peaks normalized to intensities mentioned in the JCPDS data file (file No. 36-1451). The last term was omitted for all samples not showing the 002 peak.

As shown in Table I, the δ_{avg} value for as-grown ZnO was calculated as 5.40×10^{10} cm^{-2} and decreased to 3.49×10^{10} cm^{-2} after nitrogen doping. As expected, both types of annealing result in lowering of the FWHM of the XRD reflections and, consequently led to the further decrease of the δ_{avg} value to the values 1.40×10^{10} cm^{-2} and 2.88×10^{10} cm^{-2}, for O_2 and N_2 RTP annealing, respectively.

4. Scanning electron microscopy and low-temperature cathodoluminescence (LT CL)

The post-RTP films showed intensive low-temperature cathodoluminescence (LT CL) in the excitonic region, i.e., in the photon energy of 3.2–3.4 eV (Fig. 2), while defect-related luminescence was not observed. Two CL bands were observed, one at 3.31 eV and the second at 3.355 eV.

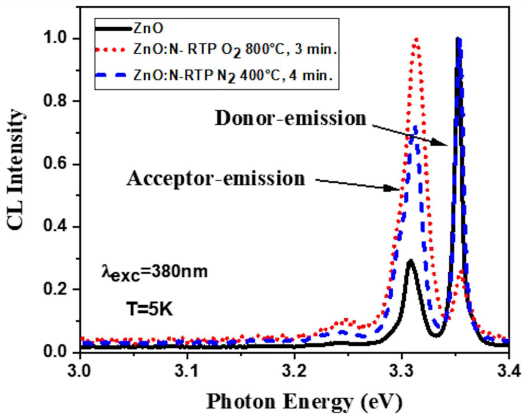

Fig. 2. Low temperature CL spectra of ZnO, ZnO:N annealed in O_2 at 800°C for 3 min and ZnO:N annealed in N_2 at 400°C for 4 min.

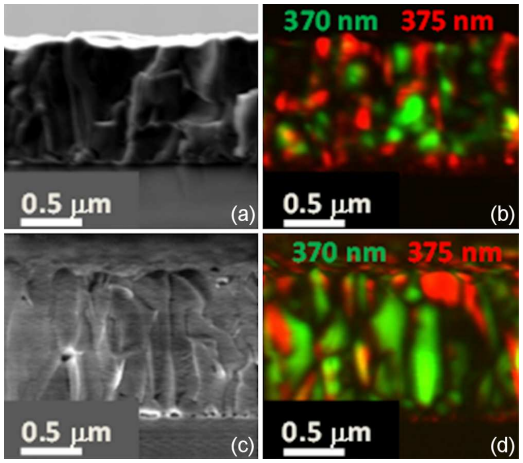

Fig. 3. Cross-sectional SEM image and LT CL map of films annealed in O_2 at 800°C for 3 min (ZnO (a, b) and ZnO:N (c, d)).

Based on the temperature-dependent photoluminescence investigations, the former line has been assigned to the free-to bound transition (FA) with the acceptor binding energy of ~ 120 meV, and the second to donor-bound exciton recombination (D^0X) center [21].

In CL spectra measured from the macroscopic surface area of the films, acceptor-related luminescence dominates in the ZnO:N film annealed with oxygen while donor-related luminescence is more intensive in the case of undoped ZnO films, as shown in Fig. 2. Nitrogen annealing of ZnO:N enhances the acceptor-related emission as compared to ZnO, but not so much as for oxygen annealing, while the donor-related emission remains unchanged. SEM images taken on the films cross-sections confirm the polycrystalline structure of the layers as shown in Fig. 3a, 4a and 5a.

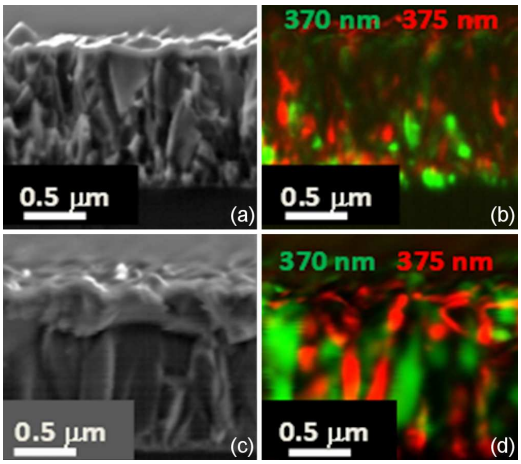

Fig. 4. Cross-sectional SEM image and LT CL map of films annealed in N_2 at 400°C for 4 min (ZnO (a, b) and ZnO:N (c, d)).

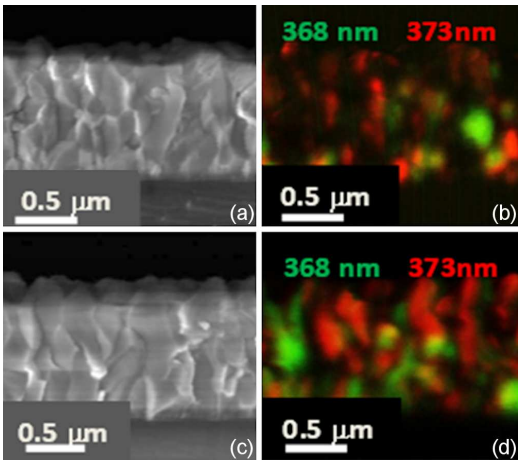

Fig. 5. Cross-sectional SEM image and LT CL map of films annealed in O_2 at 800°C for 3 min (a, b) and 6 min (c, d) for ZnO:N films.

Cross-sectional SEM images (gray) have been compared to the LT CL images taken at 5.3 K and recorded from exactly the same region where the donor-related emission is shown in green, while the acceptor-related luminescence is shown in red (Figs. 3, 4, 5).

A comparison of SEM and LT CL images of ZnO and ZnO:N films reveals that acceptor and donor-related emissions derive from micro-regions of the samples related to crystallites. In the ZnO films, annealed in O_2, acceptor and donor-related regions are randomly distributed over cross-section of the film (Figs. 3b and 4b), but in the case of annealed ZnO:N, the regions of acceptor emission seem to be oriented along the columns of the growth (Figs. 3d and 4d). As can be seen in all LT CL images, the area of acceptor-related CL is comparable to the area of donor-related CL, so the acceptor luminescence does not originate from grain boundaries.

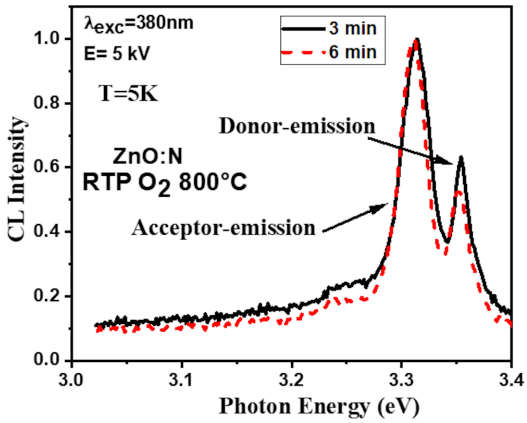

Fig. 6. Low temperature CL spectra of ZnO:N annealed in O_2 at 800°C for 3 min and 6 min.

This conclusion is confirmed by the XRD studies, which show an increase of crystallite size and a decrease of the average dislocation density after nitrogen doping and post-growth annealing. The results of the present study are different than that reported by Schirra et al. [15] where the acceptor-related CL measured on cross-section of the epitaxial ZnO was found to originate from staking faults. The stacking faults problem focused a lot of scientific attention in the past few years [15, 22, 23] where spatially resolved CL studies revealed that in epitaxial ZnO films the 3.31 eV emission line ascribed to acceptors is related to the lines of structural imperfections that question the possibility of obtaining acceptor conductivity with carriers mobility high enough for electronic applications. The differences between the present results and those reported before can be understood in terms of different growth conditions. For the experiment reported here, ZnO and ZnO:N films were deposited under oxygen-rich conditions, which facilitate the formation of zinc vacancies that, according to present understanding, are necessary for the creations of $V_{Zn}N_O$ and $V_{Zn}N_OH$ complexes responsible for macroscopically observed hole conductivity of ZnO:N.

Additionally, the performed studies show that acceptor-related CL is more intensive in the case of annealing in oxygen at 800°C than in nitrogen (compare Fig. 4b and d). Moreover, prolonged RTP annealing in oxygen (6 min) may further enhance the area of the acceptor-related CL (compare Fig. 5b and c), while the shape of CL spectra is almost similar (Fig. 6). One important fact to be mentioned here is that samples shown in Figs. 3d and 5b are grown in similar conditions but different ALD processes. It should also be remembered that LT CL images are slightly different for these samples because CL measurements need a freshly cleaved cross-sectional area for an experiment and every cleavage is a bit different even for the same sample. Also, the contrast of the CL maps might be slightly different.

5. Conclusions

We deposited 2 μm thick polycrystalline ZnO and ZnO:N films by ALD under O-rich conditions (at 100°C). Post-growth annealing was done at different ambience and temperature to achieve intensive LT CL. Comparison of SEM and LT CL images of ZnO and ZnO:N films reveal that the acceptor and donor-related emissions are clearly separated and originate from different micro-crystallites present on the film cross-section. In the case of ZnO:N annealed in oxygen, the acceptor-related emission regions are gathered along the columns of growth, while they were randomly distributed over the cross-section of the film for undoped samples. In the CL spectra taken at the macroscopic surface region, the results of which can be compared with the PL spectra, the acceptor-related luminescence dominates in the ZnO:N film annealed in oxygen, while the donor-related luminescence is more intensive for undoped ZnO films. XRD confirms that grain size increases and dislocation density decreases after nitrogen doping and RTP annealing, so we are able to report that the enhancement of the acceptor-related emission is not due to grain boundaries or staking faults. Annealing in oxygen at 800°C (3 min) results in more intensive acceptor-related CL than annealing in nitrogen ambience, and prolonged annealing in oxygen at 800°C (6 min) additionally increases it.

Acknowledgments

The work was supported by the Polish National Centre Project DEC-2018/31/B/ST3/03576.

References

[1] C. Lee, S.Y. Park, J. Lim, H.W. Kim, *Mater. Lett.* **61**, 2495 (2007).

[2] D.C. Look, B. Claflim, Ya.I. Alivov, S.J. Park, *Phys. Status Solidi (a)* **201**, 2203 (2004).

[3] T.A. Krajewski, K. Dybko, G. Łuka, E. Guziewicz, P. Nowakowski, B.S. Witkowski, R. Jakieła, L. Wachnicki, A. Kamińska, A. Suchocki, M. Godlewski, *Acta Mater.* **65**, 69 (2014).

[4] D.M. Hofmann, A. Hofstaetter, F. Leiter, H. Zhou, F. Henecker, B.K. Meyer, *Phys. Rev. Lett.* **88**, 4 (2002).

[5] X.L.Wu, G.G. Siu, C.L. Fu, H.C. Ong, *Appl. Phys. Lett.* **78**, 2285 (2001).

[6] E. Guziewicz, E. Przezdziecka, D. Snigurenko, D. Jarosz, B.S. Witkowski, P. Dłużewski, W. Paszkowicz, *ACS Appl. Mater. Interfaces* **9**, 26143 (2017).

[7] A. Janotti, C.G Van de Walle, *Rep. Prog. Phys.* **72**, 126501 (2009).

[8] C.G. Van de Walle, D.B. Laks, G.F. Neumark, S.T. Pantelides, *Phys. Rev. B* **47**, 15 (1993).

[9] J.L. Lyons, A. Janotti, C.G. Van de Walle, *Appl. Phys. Lett.* **95**, 252105 (2009).

[10] C.H. Park, S.B. Zhang, S.H. Wei, *Phys. Rev. B: Condens. Matter Mater. Phys.* **66**, 073202 (2002).

[11] M.N. Amini, R. Saniz, D. Lamoen, B. Partoensa, *Phys. Chem. Chem. Phys.* **17**, 5485 (2015).

[12] L. Liu, J. Xu, D. Wang, M. Jiang, S. Wang, B. Li, Z. Zhang, D. Zhao, C.X. Shan, B. Yao, D.Z. Shen, *Phys. Rev. Lett.* **108**, 215501 (2012).

[13] D.Y. Yong, H.Y. He, Z.K. Tang, S.-H. Wei, B.C. Pan, *Phys. Rev. B* **92**, 235207 (2015).

[14] D. Snigurenko, K. Kopalko, T.A. Krajewski, R. Jakieła, E. Guziewicz, *Semicond. Sci. Technol.* **30**, 015001 (2015).

[15] M. Schirra, R. Schneider, A. Reiser, G.M. Prinz, M. Feneberg, J. Biskupek, U. Kaiser, C.E. Krill, K. Thonke, R. Sauer, *Phys. Rev. B* **77**, 125215 (2008).

[16] S. Mishra, E. Przezdziecka, W. Wozniak, A. Adhikari, R. Jakiela, W. Paszkowicz, A. Sulich, M. Ozga, K. Kopalko, E. Guziewicz, *Materials* **14**, 4048 (2021).

[17] E. Przezdziecka, E. Guziewicz, D. Jarosz, D. Snigurenko, A. Sulich, P. Sybilski, R. Jakiela, W. Paszkowicz, *J. Appl. Phys.* **127**, 075104 (2020).

[18] P. Gay, P.B, Hirsch, A. Kelly, *Acta Crystallogr.* **7**, 41 (1954).

[19] G.K.Williamson, R.E. Smallman, *Philos. Mag.* **1**, 34 (1956).

[20] S.B. Ameur, H.B. Hadjltaief, A. Barhoumi, B. Duponchel, G. Leroy, M. Amlouk, H. Guermazi, *Vacuum* **155**, 546 (2018).

[21] E. Przezdziecka, E. Guziewicz, B.S. Witkowski, *J. Lumin.* **198**, 68 (2018).

[22] K. Thonke, M. Schirra, R. Schneider, A. Reiser, G.M. Prinz, M. Feneberg, J. Biskupek, U. Kaiser, R. Sauer, *Microelectron. J.* **40**, 210 (2009).

[23] B. Sieber, A. Addad, S. Szunerits, R. Boukherroub, *J. Phys. Chem. Lett.* **1**, 3033 (2010).